

Optimization of a RSD X-Ray Backscatter System for Detecting Defects in the Space Shuttle External Tank Thermal Foam Insulation

Daniel Shedlock*, Benjamin Addicott, Edward T. Dugan, and Alan M. Jacobs
Nuclear & Radiological Engineering, 202 NSC, Box 118300,
University of Florida, Gainesville, FL 32611;

ABSTRACT

A new Compton x-ray backscatter imaging technique, backscatter radiography by selective detection (RSD), has been used for inspection of the spray-on-foam-insulation (SOFI) on the space shuttle external tank. RSD employs detection of selected backscatter field components, by using specially designed detectors with movable detector collimators, to achieve high image contrast.

The optimization study utilized test panels with simulated and natural defects in the spray-on foam insulation. Some of the test panels include structural features, stiffener-stringers and connection flanges, which were bolted to an aluminum base plate representative of the external tank. The SOFI was then layed down over the base plate and structural components with thicknesses varying from a few tens of mm up to a few hundred mm. The simulated defects range in cross-sectional size from 6 x 6 mm to 50 x 50 mm. Natural defects including roll-over voids and knit-line delaminations have a wide range of sizes, geometries, and orientations with a minimum critical cross-sectional size of 6 mm. Imaging registration is currently obtained at 0.05 seconds per 2 mm pixel, or about 19 minutes per 0.093 m² (1 ft²).

The current system is being evaluated to enhance the detection of natural defects of a minimal critical size. Monte Carlo (MC) simulations with MCNP5 are being used to determine the history and corresponding spectrum of the detected photons that are responsible for improving defect image contrast. The simulation results are used in combination with experimental data to select optimal detector configurations. Detector configurations are sensitive not only to the type of defect being detected, but also the defect's depth in SOFI, distance from aluminum substrate, and defect orientation.

Additional parameters including detector type, detection mode, and x-ray illumination beam size were also evaluated. Both NaI and plastic (BC404) scintillation detectors in pulse and integral mode were used to determine their effect on image quality and defect detection sensitivity. The x-ray illumination beam geometry (round versus square) and beam spot size were varied to determine resolution and the effect on defect contrast. The current system using pulse mode NaI detectors, and a 2 mm round x-ray illumination beam can detect the presence of the smallest critical size defects at a scan rate of 0.05 seconds per 2 mm pixel.

Keywords: Flaw and defect detection, backscatter x-ray imaging, delaminations, lateral migration radiography, selective detection.

* shedlock@ufl.edu; phone (352) 392-1401 (ext 344); fax (352) 392-3380

1. INTRODUCTION

1.1. X-ray Backscatter Radiography by Selective Detection

Radiography by selective detection (RSD) is a new type of x-ray Compton backscatter imaging (CBI) where different components of the x-ray backscatter field are preferentially selected to enhance the contrast and detection of specific features. A variant of this technique, called lateral migration radiography (LMR), was first applied at the University of Florida (UF) to the detection of buried land mines¹⁻¹⁰. The land mine results demonstrated the ability of this technique to detect voids, and air spaces. As a result, RSD was applied to the detection of subsurface features including: cracks, voids, delaminations and corrosion. A wide variety of materials have been imaged including: aluminum, plastics, honeycomb structures, laminates¹¹, steel, reinforced carbon-carbon composites (RCC), concrete, and titanium. Most recently, an RSD scanning system is being used by Lockheed Martin Space Systems Co. and NASA to detect defects in the spray-on foam insulation (SOFI) used on the external fuel tank of the space shuttle¹².

The x-ray backscatter radiography by selective detection approach is based on image contrast induced by varying electron densities along the photon path. Changing subsurface features cause photons to be scattered, absorbed or stream along their path to the detector. Each of these interactions results in changes in the detector response. These changes in detector response are collectively used to generate an image, where changes in field intensity (count rate or voltage) are visually represented as changes in image contrast. Backscatter RSD selectively detects x-rays that enhance the signal-to-noise ratio allowing for the detection of features, which may otherwise go undetected using conventional CBI or transmission radiography. Figure 1 illustrates how a combination first- and multiple- scatter events from various scan depths, can be used to image a variety features at different depths. Subsurface features can be anything of interest: cracks, corrosion, voids, delaminations, land mines, hidden objects, or improvised explosive devices (IEDs).

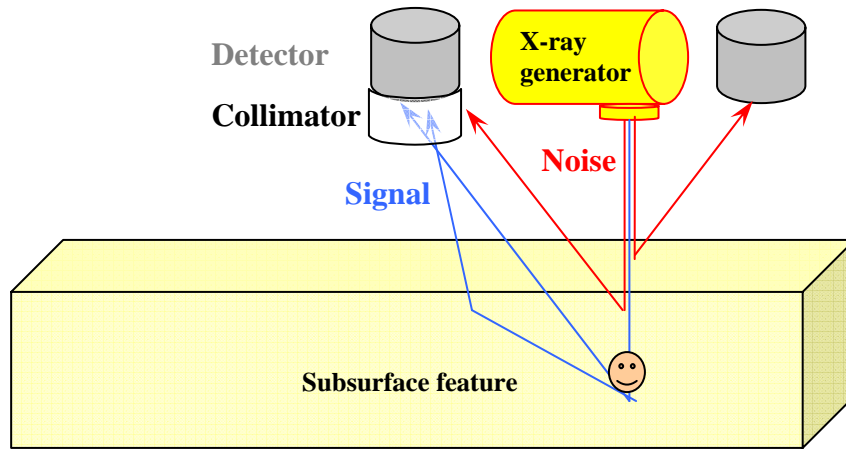


Figure 1 - Simplified Schematic of a RSD Subsurface-Feature Experimental Setup with a Collimated Detector

1.2. RSD Scanning System

In general, as shown in Figure 2 the current RSD scanning system consists of the x-ray generator, an array of detectors, scanning table, and a computer to control data acquisition, motion control, and image generation. The array of detectors is fixed to the x-ray generator and designated as the scanning head. A highly collimated x-ray beam illuminates a single pixel, and a selective backscatter field is measured by the array of detectors. Movable collimators allow each of the

detectors to view a unique field. The measured signal of less collimated, or uncollimated detectors is dominated by single-collision events and contains surface and near surface information. The collimated detector signals can respond to single- and multiple-scatter photons. These photons have greater depth penetration and carry information about sub-surface features. Two dimensional images are generated using a scanning pattern. For example, the scanning head will sweep from left to right, acquiring data and storing a line of pixels. The scanning head will then move to the next line and sweep in the opposite direction from right to left, obtaining the next line of data. This process is repeated one line at a time until the entire image is completed.

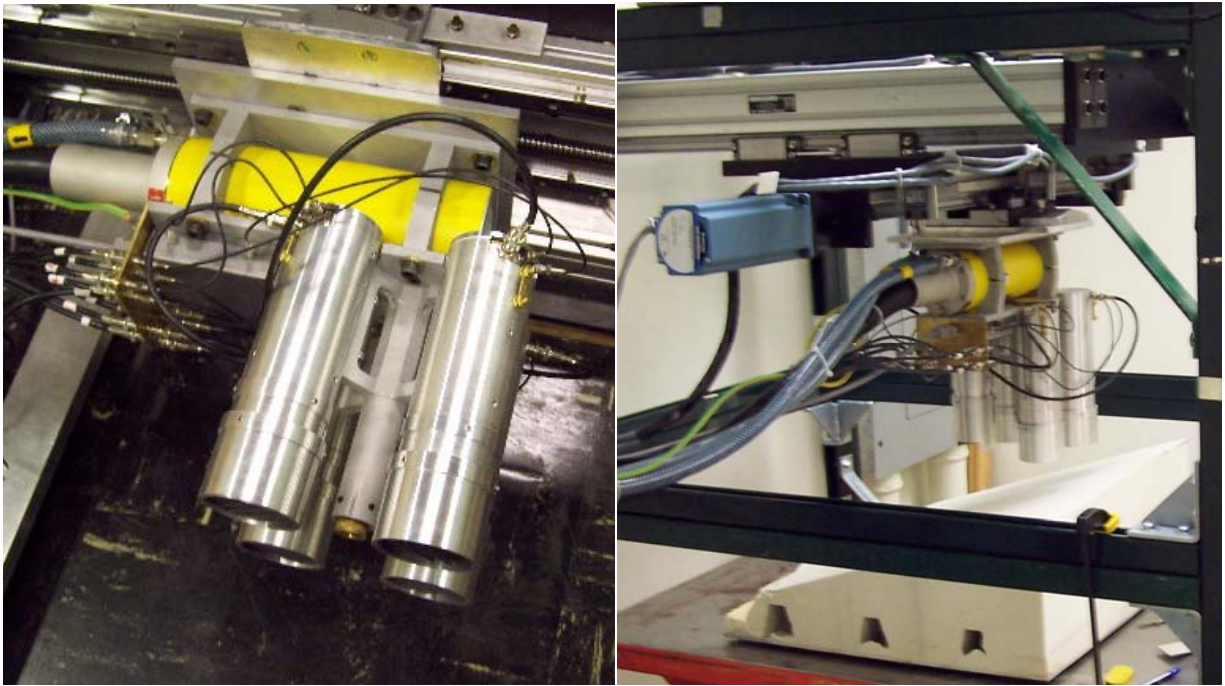


Figure 2- Current RSD Scanning System Configuration

The scanning system in Figure 2 is used for examining the spray-on foam insulation (SOFI) on the external tank of the space shuttle. The yellow cylinder is an Yxlon MXR-160/22 x-ray generator. This is a liquid-cooled x-ray generator with a maximum tube voltage of 160 kV. For the thermal foam insulation application, the tube voltage used is nominally 60 kV. The maximum tube current at this voltage is 45 mA with a 5.5 mm focal spot. For the foam thermal insulation examination, the tube current used is typically about 45 mA. The four silver cylinders in Figure 2 are the detector assemblies. Each detector assembly includes a 50 mm diameter by 50 mm long NaI scintillator crystal, a photomultiplier tube and a specially-designed, high speed, ultra low-noise pre-amplifier. The collimator assembly at the end of the detector includes an array of lead collimators and the design allows for independent adjustment of the assembly in different directions. This includes in-and-out movement of the outer, circular (sleeve) collimator; in-and-out and rotational movement of the inner collimator (collimator component with the lead fins); and in-and-out movement of the entire assembly. The collimator design provides the ability to “focus” the image by the selection of the desired scatter components. Each of the detectors generates a separate image and a cross-correlated image can also be generated from any combination of detector images. The x-ray illumination beam spot size used is typically 2 mm for first pass scan, and 1 mm for suspect areas or areas of interest. The beam spot is usually either round or square, but can be customized for any application. The shape of the illumination beam is controlled by a lead insert in the bottom of the brass, lead-lined source collimator tube that extends in a direction normal to the end of the x-ray tube and which is centered between the four detectors. The fastest linear scan rate for this system is about 50 mm per second. For 2 mm pixels, this

translates into scanning rate of approximately 15 minutes per 0.093 m² (1 ft²). A LabVIEW-based program is used to control the scanner motion, data acquisition and image generation.

1.3. Spray-on Foam Insulation

Spray-on foam insulation (SOFI) is a low density insulation (0.03 g/cm³) that is applied to the external tank of the space shuttle to prevent the buildup of ice. The foam is applied in layers and is susceptible to subsurface defects which may weaken the integrity of the foam causing it to tear-off during launch. To reduce the risk associated with these defects, “areas of interest” are inspected using x-ray backscatter RSD and terahertz¹³ imaging. As shown in Figure 3, some of the areas of interest include: the bipod area where the nose of the orbiter attaches to the external tank, the protuberance air load (PAL) ramp, which protects the tank cable trays and pressurized lines, and the flange area where the liquid hydrogen and oxygen tanks bolt together.

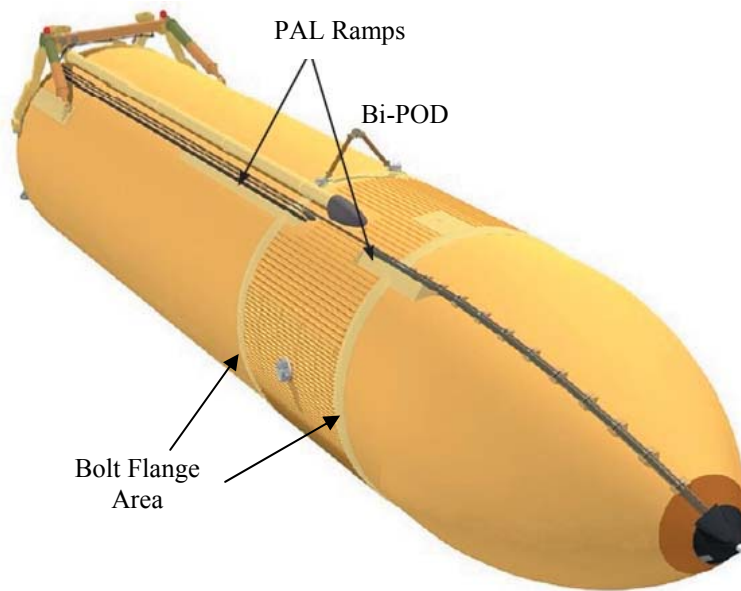


Figure 3- Areas of Interest for Defect Inspection

2. RESULTS and DISCUSSION

2.1. Detector Response to Collimator Variations

The Monte Carlo N-Particle (MCNP5) Transport code system was used to model NaI detector response to changes in detector collimator length and sample-to-detector spacing. Detector collimators are one method the RSD scanning system uses to preferentially select backscatter photons that enhance image contrast as desired. The MCNP model used for these calculations is shown in Figure 4. The spray-on foam insulation is 203.2 mm thick on an aluminum substrate as shown in Figure 4. The SOFI is divided into four equal 50.8 mm layers for tallying purposes only. The detector collimator is 1.6 mm thick lead. The detector is 50.8 mm in diameter and 50.8 mm thick. The vertical centerline of the detector is located 203.2 mm from the illumination beam. Calculations were performed for different x-ray peak energies of 45 kVp, 60 kVp, and 75 kVp. The 60 kVp illumination spectrum¹⁴ shown in Figure 5 is calculated based on an

electron beam impinging on a tungsten target. The exact composition of the SOFI insulation is proprietary, and only the components are known. However, in order to develop a MCNP model, the composition and concentrations were assumed to be similar to industrial spray-on foam insulation. Dow Ethafoam at a density of 0.03 g/cm^3 is similar in composition to SOFI and consists primarily of carbon (28.6%), nitrogen (5.7%), oxygen (8.6%), and hydrogen (57.1%).

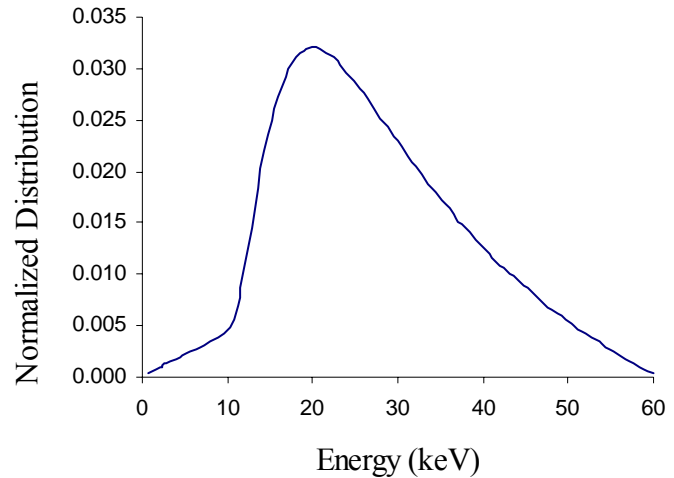
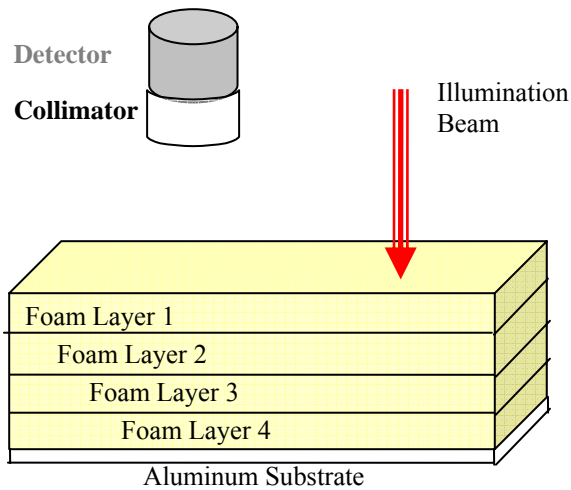


Figure 4 – Sketch of MCNP Model Geometry

Figure 5 – MCNP Source Illumination Spectrum 60 kVp

Monte Carlo results indicate that the average mean free path (MFP) of the x-rays in the SOFI are extremely large compared to the aluminum substrate. As given in Table 1, the average MFP for x-rays with a 60 kVp spectrum is about 92 cm. As a result, a large number of photons are backscattered off the aluminum substrate as shown in Figure 6. Figure 6 summarizes each layer’s percent contribution to the detector response for a 60 kVp illumination spectrum.

For brevity, discussion will be focused on the 60 kVp results. The external tank is currently scanned at 55-60 kVp because this energy provides the best image contrast for naturally occurring defects. For the first simulation, the face of the NaI detector was located 11.4 mm from the surface of the SOFI and the collimator was flush. About 26% of the backscatter signal is penetrating to the aluminum substrate and the contributions from layers 1 through 4 are 23%, 25%, 16%, and 10% respectively. Fortunately, even photons that penetrate to aluminum need to transverse the layers of foam on the penetrating and return path to the detector. As a result, changes in the foam along the backscatter path will affect the backscatter field and result in a change in image contrast. It should be noted the layer 1 contribution (23%), is slightly less than the layer 2 contribution to the signal (25%). This is expected, because the illumination beam is located 63.5 mm from the edge of the detector. With the detector located only 11.4 mm from the surface of the foam, the solid angle from the detector surface to beam is larger for layer 2, hence increasing the layer 2 contribution.

Table 1 – MCNP Estimates of Average MFP of X-rays in SOFI and Aluminum

Material	45 kVp	60 kVp	75 kVp
SOFI	660 mm	920 mm	1100 mm
Aluminum	3.3 mm	5.7 mm	8.1 mm

For the second or middle data set in Figure 6, the distance between the surface of the SOFI and the detector face was increased to from 11.4 mm to 51.4 mm, and the detector collimator remained flush. The results of this simulation are similar to the results from the first simulation, except the solid angle between layer 1 and detector has increased, and

layer 1 contributes almost 30% to the detector response. Contributions from each of the remaining deeper layers only decrease slightly. This geometry would be a preferred geometry for detecting defects in layer 1. For the third calculation, the detector to sample distance remained at 51.4 mm, and the lead collimator sleeve was extended 40 mm beyond the face of the detector toward the foam sample. With a 40 mm collimator extension, x-rays must penetrate to a depth of at least 50 mm into the SOFI to be backscattered into the detector (depth calculated based on 1st scatter solid angle). As a result, the contribution to detector response from layer 1 has dropped to about 1%. The layer 2 contribution was reduced from 22% to 16%, and the contributions from layers 3 and 4 were increased to 20% and 17%, respectively. The contribution from the aluminum for this configuration is nearly half of the measured signal at 46%. However, x-rays which have penetrated to deeper layers, must transverse the more shallow layers on the entrance and exit paths. Material structure, and features from these shallow layers will affect the transport of deeper penetrating x-rays. This allows scatter components reflecting from the aluminum substrate to contribute a detectable signal that includes information about subsurface features in the foam.

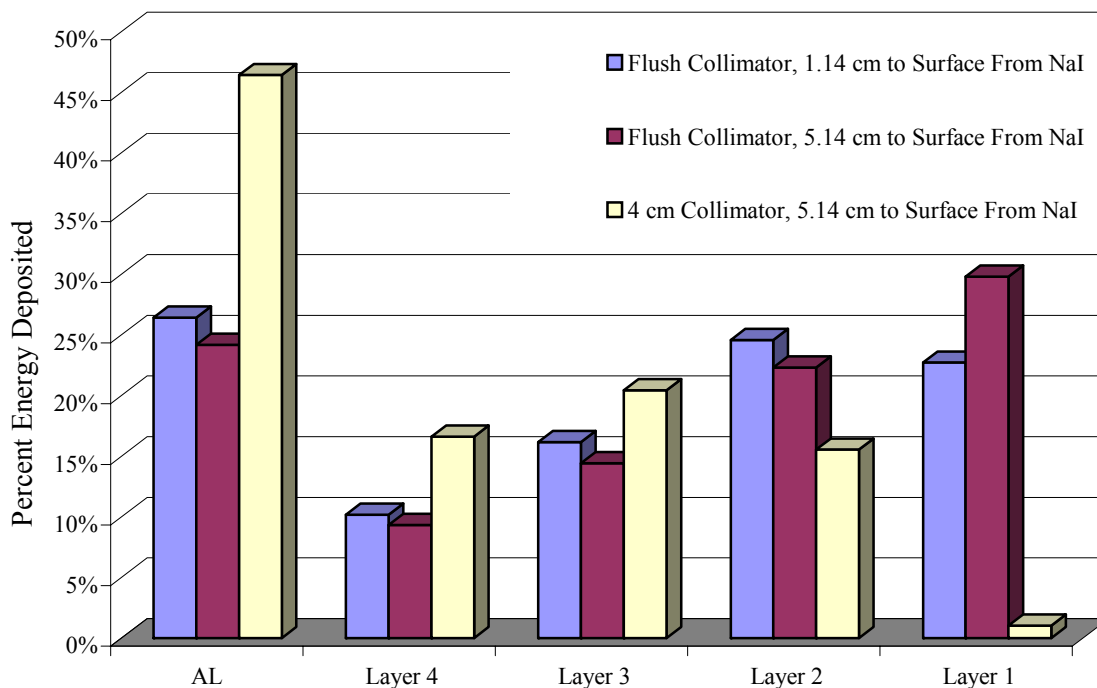


Figure 6 – Detector Energy Deposition by Cell, 203.2 mm of SOFI on Al Substrate (60 kVp)

2.2. Illumination Beam Aperture Geometry

Extending downward in a direction normal to the x-ray tube is the illumination beam collimator. The illumination beam size and geometry can be varied by changing a lead disk aperture where the x-ray beam exits the collimator tube. Originally circular apertures were used to illuminate a single pixel as shown in Figure 7. However, image pixels are square and a square aperture increases the illumination beam intensity by a factor of $4/\pi$ (1.27 times). The larger beam area and intensity results in a higher count rate, and reduces image acquisition time. Also note that as shown in Figure 7 the illumination beam is chosen slightly smaller than the pixel area. For example, to generate an image with 2 mm pixels, it is recommended to use a 1.5 mm aperture. This reduces pixel cross illumination due to beam dispersion and helps to improve image quality. Figure 8 quantifies the illumination beam dispersion at 101.6 mm from the beam exit aperture. A pixel size of 2.5 mm for a 2.0 mm aperture reduces pixel cross illumination to less than 5% for a round aperture and to less than 7% for the square aperture. The film exposure used to generate each plot is shown in the legend of Figure 8. To ensure the film is not over exposed, several exposures were made at 55 kVp. The x-ray current and exposure were reduced until the beam plateau dropped below 255 (pure white in an 8 bit grey scale image). The final x-ray generator settings for the film exposures were 55kVp, 0.5 mA, and a 2 second exposure.

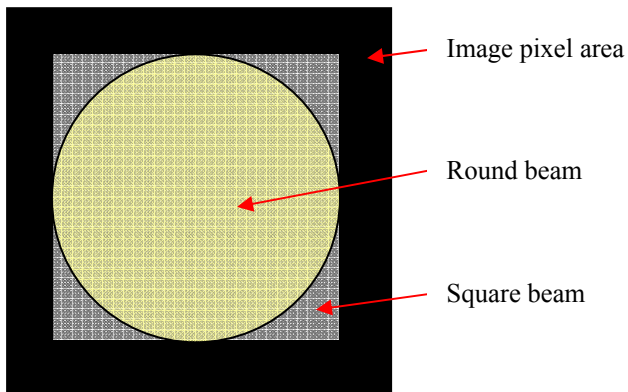
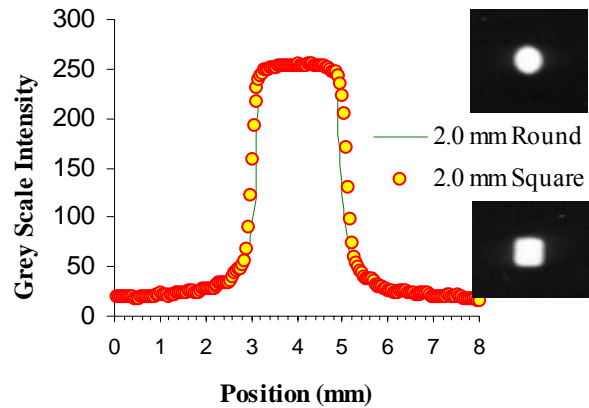


Figure 7 – Illumination Beam Aperture Geometry



**Figure 8 – Beam Dispersion Measurements
101.6 mm from Source**

2.2.1. Round and Square Aperture Images

Figure 10 is a picture of the layout used to scan a ramp panel with natural defects and debris embedded in the SOFI. The image pixel size is set at 2mm, with a pixel dwell time of 0.1 seconds per pixel. The x-ray generator settings were 55 kVp, and 45 mA with a 5.5 mm focal spot (FOC). The collimators extend at total of 15 mm past the surface of the NaI detectors, and the minimum separation distance (where foam is thickest) between the SOFI and the face of the detectors was 40 mm. The foam varies in thickness from 38.1 mm to 228.6 mm. The aluminum flange runs the length of the panel and is used to bolt the liquid hydrogen and oxygen tanks together. The stiffener-stringers lay perpendicular to the flange located in each position where the flange is bolted together.

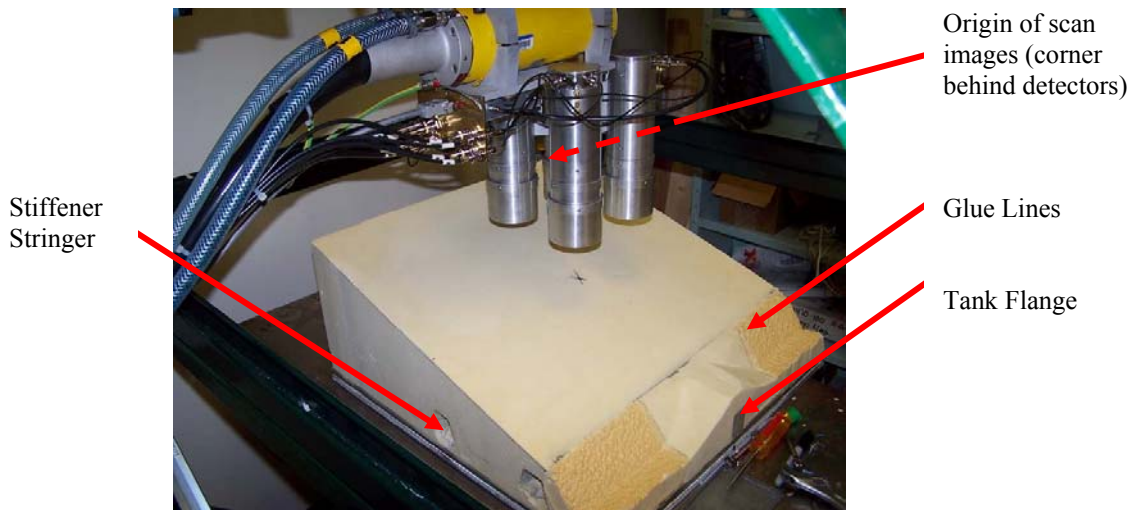


Figure 10 – Scanning Configuration for Ramp Panel

Figures 11 and 12 are RSD images of a ramp panel using a 2 mm round and square aperture, respectively. The difference in count rate is because of the change in area of the illumination beam aperture as shown in Figure 7. The

count rate for the square aperture image is approximately 1.3 times the count rate of the round aperture image as expected.

Two metal flanges run vertically in the image at $x = 250$ mm and are bolted together. The stiffeners are in the x-direction on both sides of the flange located at $y = 100$ mm, 275 mm and 460 mm. The stiffeners are bolted to the aluminum substrate. Glue lines can be seen running vertically in the image at $x = 125$ mm and $x = 375$ mm. There are five dominate natural defects in the image: defect 1 ($x = 60$, $y = 375$); defect 2 ($x = 90$, $y = 180$); defect 3 ($x = 450$, $y = 375$); defect 4 ($x = 150$, $y = 15$); and defect 5 ($x = 400$, $y = 25$). There are four items of floor debris easily visible in the image: debris 1, tape ($x = 175$, $y = 180$); debris 2, pencil ($x = 250$, $y = 375$); debris 3, nylon washer ($x = 350$, $y = 375$); and debris 4, bolt ($x = 360$, $y = 165$). The count rate in the images has a decreasing trend from bottom to top due to the increasing thickness of the foam.

The images in Figures 11 and 12 were imaged using round and square apertures equal to the image pixel size (2 mm). This example demonstrates how aperture size can affect image contrast. The absolute signal contrast for natural defect 4 is 5.2 % for the round aperture, and 4.0 % for the square aperture. The reduction in image contrast can be partially attributed to pixel cross illumination. The illumination beam aperture should be slightly smaller than the image pixel size for square apertures, and smaller or equal size for round apertures.

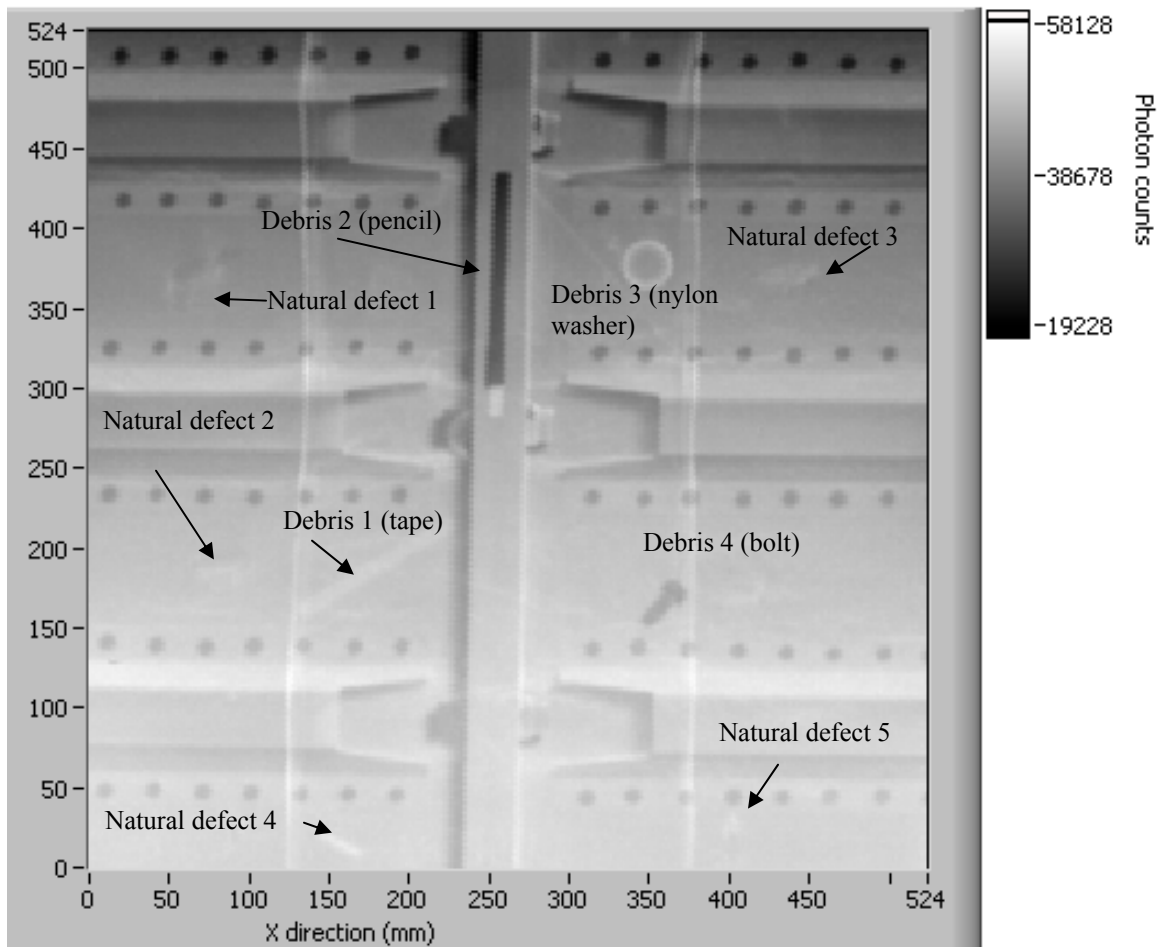


Figure 11 – 2 mm Round Aperture Ramp Panel Image (55 kVP)

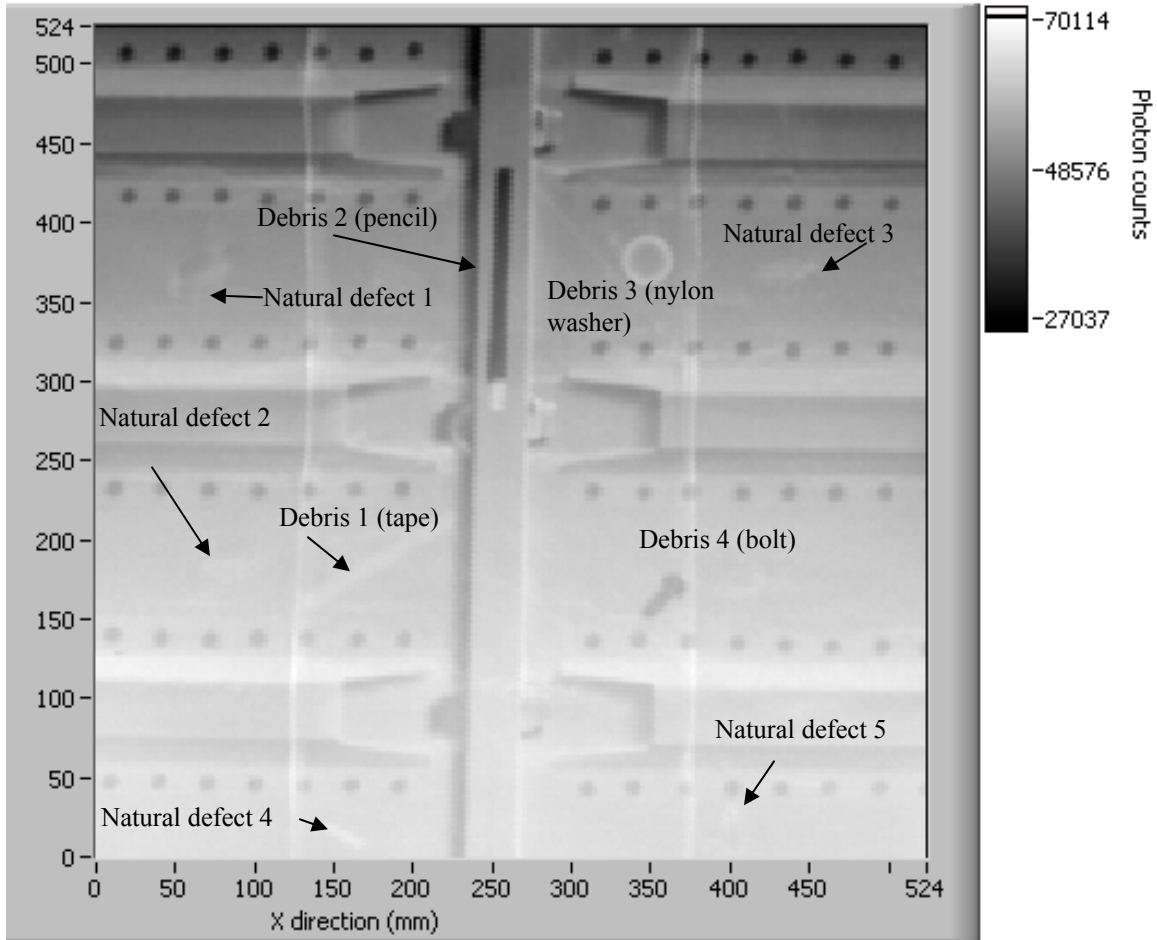


Figure 12 – 2 mm Square Aperture Ramp Panel Image (55 kVP)

Detector Modifications

2.2.2. Detector Preamp Modifications

The current systems in use for inspection of the external tank uses a set of four NaI detectors in pulse counting mode to measure the x-ray backscatter field. Typical pulse counting preamps have relatively long time constants, which results in pulse widths of several micro-seconds. Customized, ultra-low-noise, high count rate preamps have been designed for the RSD scanning systems. These preamps have a maximum noise level of about 5 mV for a 1 volt pulse output, while operating in close proximity to a strong electro-magnetic field (x-ray generator tube). The preamp pulses have a typical rise time of 100 nano-seconds and fall time of about 1000 nano-seconds, yielding a total pulse width of about 1.1 micro-second. This specific pulse width (1.1 micro-seconds) allows sufficient light and charge collection time from the NaI and PMT (about five time constants), while allowing the detectors to measure backscatter fields up to 700,000 counts per second, without experiencing statistically significant pulse pile-up. The RSD scanning system utilizes these ultra-low noise, high count rate preamps to reduce scan time by decreasing the count time per unit pixel required to reach an acceptable level of statistical counting uncertainty. The original preamps used on the system had a pulse width of 2.2 micro-seconds; therefore, the redesigned preamp allows for a theoretical speedup in scan time by a factor of two, while maintaining the same level of statistical noise on a per pixel basis. Because of the nature of backscatter radiography by selective detection, only a small fraction (typically less than 0.1%) of the original illumination beam contributes to the

measured signal. In some scanning figurations, depending on material and geometry, the limiting x-ray tube current setting and illumination beam intensity is reached (45 mA) before reaching the upper counting limit of 700,000 count per second. All count rate images in this paper were generated using the ultra-low-noise, high count rate preamps.

2.2.3. Current Mode Versus: Counting Mode Detectors

Current mode detectors generate an analog voltage/current output that is proportional to the count rate and energy deposition, while count mode detectors generate a voltage pulse for which the height of the pulse is proportional to deposited energy. However, for the RSD scanning system, image pixel contrast was generated based on count rate, and each count was equally weighted regardless of pulse height. An image data file simply consists of an array of integers (counts per pixel). The range of integer numbers is then linearly scaled to a 16 bit range (0 to 65,536) where the lowest count is mapped to zero and the highest count is scaled to 65,536. When a detector is operating in current mode, the RSD scanning system measures the analog voltage signal, the 0 to 5 volts voltage signal is then linearly scaled to a 16 bit range. When measuring the analog signal, the image contrast is affected by the energy of the radiation that is incident on the detector. As a result, the image contrast is weighted toward higher energy backscatter x-rays, because higher energy x-ray induce a higher voltage, but not a higher count rate. Figures 13 and 14 are SOFI calibration block images. There are two small cylindrical voids, 6.35 mm in diameter and height, and two large cylindrical voids, 12.7 mm in diameter and height. The shallow voids in the bottom of each image are located under 50.8 mm of foam and the deeper voids are near the aluminum substrate beneath 203.2 mm of foam. Absolute percent signal contrast between the void and background was calculated for the 12.7 mm voids. The current mode detector has a defect-to-background contrast variation of 5.7 % and 3.2 % for the shallow and deep voids respectively, while the pulse (count) mode detector measures a defect-to-background contrast of 4.0 % and 2.0 % for the shallow and deep voids.

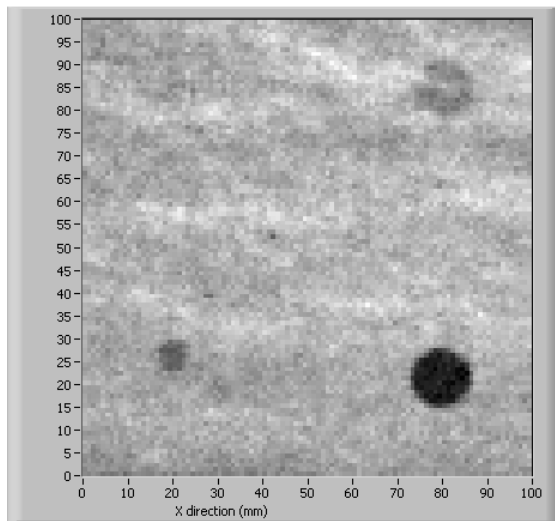


Figure 13 – Foam Calibration Block (Current Mode)

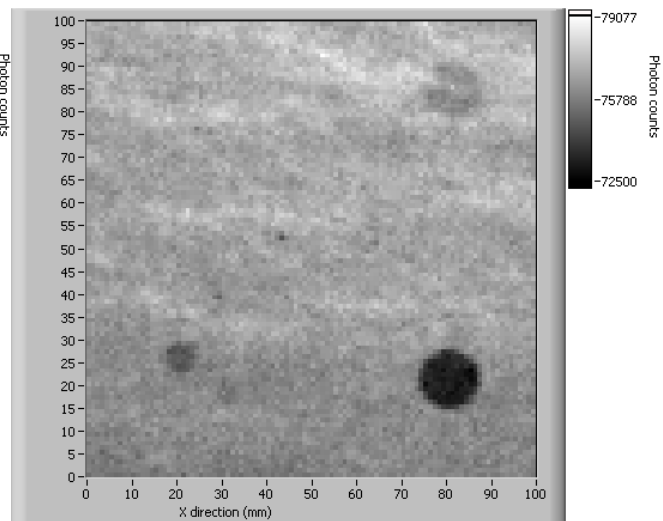


Figure 14 – Foam Calibration Block (Pulse Mode)

2.2.4. Comparison of NaI and Plastic (BC404) Scintillation

The current RSD system NaI detectors are 50.8 mm in diameter and 50.8 mm thick. Although a much thinner NaI crystal (6.35 mm thick) is adequate, 50.8 mm thick crystals were more readily available off-the-self. Plastic (BC404) scintillator detectors were tested in comparison to the NaI detectors, because plastics have a much faster decay time, and could in theory measure higher radiation fields. The plastic detectors tested also had a 50.8 mm diameter, 50.8 mm thick active detection volume, and used 1.1 micro-second pulse width preamplifiers in count mode. However, plastic detectors

were about 30% less efficient than NaI detectors. As a result the count rate on the plastic detectors was about 2/3 of the count rate of the NaI detectors. A lower count rate resulted in images with less contrast in comparison to the NaI detectors and potentially longer image acquisition times. Plastic detectors should be investigated in a current mode configuration.

3. CONCLUSIONS

Radiography by selective detection (RSD) preferentially selects x-ray backscatter field components to enhance the contrast and detection of specific features. Acquired images have clearly shown, for a variety of conditions, that proper selection of x-ray field scatter components leads to a significant improvement in image quality and contrast, so much so that in some cases objects that are not visible in conventional CBI become readily discernable. The system has been used to detect cracks, voids, delaminations and corrosion in a wide variety of material including: aluminum, plastics, honeycomb structures, laminates, steel, reinforced carbon-carbon composites (RCC), concrete, and titanium.

Most recently, RSD scanning systems are being used by Lockheed Martin Space Systems Co. and NASA to detect defects in the spray on foam insulation (SOFI) used on the external fuel tank of the space shuttle. Because of the properties of the foam thermal insulation, including its extremely low density (~0.03 g/cc), detection of flaws and defects in this material is a very difficult technical problem. The results and improvements presented herein demonstrate the very successful performance of RSD in this challenging application.

Recent improvements to the system include: customized, ultra-low-noise, high count rate preamps that can handle count rates up 700,000 cps, the addition of square beam illumination apertures to the existing set of round apertures, and the capability to utilize either current mode and/or count mode detectors. These improvements allow for faster scan times, improved image contrast, and additional versatility. MCNP models have been developed to assist in the understanding of the interaction processes governing the RSD backscatter imaging. These calculations provide insight in determining optimum RSD settings for enhancing image contrast.

ACKNOWLEDGMENTS

This material is based upon work supported by Lockheed Martin Space Systems Co.

PROPRIETARY AND PATENT CONSIDERATIONS

Portions of this work related to radiography by selective detection of scatter field velocity components, including the detector and detector collimator systems used to achieve this imaging modality, are covered by a pending U.S. Patent titled "Radiography by Selective Detection of Scatter Field Velocity Components," that has been submitted through the University of Florida Office of Technology Licensing.

REFERENCES

1. S. Campbell, and A. Jacobs, "Detection of Buried Land Mines by Compton Backscatter Imaging," *Nuclear Science and Engineering*, **110**, pp. 417-424, 1992.

Y. Watanabe, J. Monroe., S. Keshavmurthy, A. Jacobs, and E. Dugan, "Computational Methods for Shape Restoration of Buried Objects in Compton Backscatter Imaging," *Nuclear Science and Engineering*, **122**, pp. 55-67, 1996.
2. J. Wehlburg, S. Keshavmurthy, E. Dugan, and A. Jacobs, "Geometric Considerations Relating to Lateral Migration Backscatter Radiography (LMBR) as Applied to the Detection of Landmines," *SPIE Proceedings on Detection and Remediation Technologies for Mine and Minelike Targets II*, Vol. 3079, pp. 384-393, Orlando, 1997.
3. E. Dugan, A. Jacobs, S. Keshavmurthy and J. Wehlburg, "Lateral Migration Radiography", *Research in Nondestructive Evaluation*, **10**, No. 2, pp. 75-108, 1998.
4. Z. Su, J. Howley, J. Jacobs, E. Dugan, and A. Jacobs., "The Discernibility of Landmines Using Lateral Migration Radiography," *SPIE Proceedings on Detection and Remediation Technologies for Mines and Minelike Targets III*, Vol. 3392, pp. 878-887, Orlando, 1998.
5. C. Wells, Z. Su, J. Moore, E. Dugan and A. Jacobs, "Lateral Migration Radiography Measured Image Signatures For The Detection and Identification of Buried Landmines," *SPIE Proceedings on Detection and Remediation Technologies for Mines and Minelike Targets IV*, Vol. 3710, pp. 906-916, Orlando, FL, 1999.
6. C. Wells, Z. Su, A. Allard, S. Salazar, E. Dugan and A. Jacobs, "Suitability of Simulated Landmines for Detection Measurements Using X-ray Lateral Migration Radiography," *SPIE Proceedings on Detection and Remediation Technologies for Mines and Minelike Targets V*, Vol. 4038, pp. 578-589, Orlando, 2000.
7. Z. Su, A. Jacobs, E. Dugan, J. Howley, and J. Jacobs, "Lateral Migration Radiography Application to Land Mine Detection, Confirmation and Classification," *Optical Engineering*, **39**, No. 9, pp. 2472-2479, 2000.
8. E. Dugan, A. Jacobs, Z. Su, L. Houssay, D. Ekdahl and S. Brygoo, "Development and Field Testing of a Mobile Backscatter X-ray Lateral Migration Radiography Land Mine Detection System," *SPIE Proceedings on Detection And Remediation Technologies for Mines and Minelike Targets VII*, Vol. 4742, pp. 120-131, Orlando, 2002.
9. Jacobs, E. Dugan, S. Brygoo, D. Ekdahl, L. Houssay and Z. Su, "Lateral Migration Radiography: A New X-ray Backscatter Imaging Technique," *Proceedings of SPIE 47th Annual Meeting, Symposium on Optical Science and Technology, Penetrating Radiation Systems and Applications IV*, Vol. 4786, pp. 1-16, Seattle, 2002
10. E. Dugan, A. Jacobs, L. Houssay and D. Ekdahl, "Detection of Flaws and Defects Using Lateral Migration X-ray Radiography," *Proceedings of SPIE 48th Annual Meeting, Symposium on Optical Science and Technology, Penetrating Radiation Systems and Applications V*, Vol. 5199, pp. 47-61, San Diego, 2003.
11. Jacobs, E. Dugan, S. Brygoo, D. Ekdahl, L. Houssay and Z. Su, "Lateral Migration Radiography: A New X-ray Backscatter Imaging Technique," *Proceedings of SPIE 48th Annual Meeting, Symposium on Optical Science and Technology, Penetrating Radiation Systems and Applications V*, Vol. 5199, pp. 47-61, San Diego, 2003.
12. E. Dugan, A. Jacobs, D. Shedlock and Dan Ekdahl, "Detection of Defects in Foam Thermal Insulation Using Lateral Migration Backscatter X-ray Radiography," *Proceedings of SPIE 49th Annual Meeting, Symposium on Optical Science and Technology, Penetrating Radiation Systems and Applications VI*, Vol. 5541, Denver, August, 2004.
13. Q. Chen, Zhiping Jiang , and X.-C. Zhang , "All-Optical THz Imaging," *Terahertz Spectroscopy and Application, Proceedings of SPIE 3617*, 98 (1999).
14. Dodson, Scott L. "Analytical Calculations in Support of Research on a Landmine Detection System Using Backscattered X-rays", *Master's Project Report, University of Florida, Dept. of Nuc. & Rad. Eng.*, (August 1994).